State-by-state calculations for all channels of the exotic (μ^-,e^-) conversion process

T. S. Kosmas,* Amand Faessler, and F. Šimkovic
Institut für Theoretische Physik der Universität Tübingen, D-72076 Tübingen, Germany

J. D. Vergados
Theoretical Physics Division, University of Ioannina, GR-451 10 Ioannina, Greece

(Received 28 August 1996; revised manuscript received 28 March 1997)

The coherent and incoherent channels of the neutrinoless muon to electron conversion in nuclei, $\mu^-(A,Z)\rightarrow e^-(A,Z)^*$, are studied throughout the periodic table. The relevant nuclear matrix elements are computed by explicitly constructing all possible final nuclear states in the context of the quasiparticle random phase approximation. The obtained results are discussed in view of the existing at PSI and TRIUMF experimental data for ^{48}Ti and ^{208}Pb and compared with results obtained by (i) shell model sum-rule techniques, (ii) nuclear matter mapped into nuclei via a local density approximation, and (iii) earlier similar calculations. [S0556-2813(97)01207-7]

PACS number(s): 23.40.Bw, 13.35.Bv, 21.60.Jz, 12.60.Cn

I. INTRODUCTION

The neutrinoless muon to electron conversion in the field of a nucleus,

$$\mu^- + (A,Z) \rightarrow e^- + (A,Z)^*, \tag{1}$$

is forbidden in the standard model by lepton flavor conservation and plays an important role in the study of flavor-changing neutral currents which violate muon and electron numbers [1–10]. Within the last decade, experiments at PSI [1,3,4] and TRIUMF [2] aiming at a search of μ-e conversion electrons have not yet observed such events. These experiments have, however, provided us with useful constraints for the violation of muon and electron numbers. The best upper limit on the branching ratio

$$R_{\mu e}^{\mathrm{Ti}} = \Gamma(\mu^-,e^-)/\Gamma(\mu^-,\nu_\mu) < 4.3\times 10^{-12} \tag{2}$$

has recently been set by SINDRUM II at PSI [1] by using ^{48}Ti as the target. This value is of the same order as the previous limit set at TRIUMF [2], i.e., $R_{\mu e}^{\mathrm{Ti}} < 4.6\times 10^{-12}$. This year [4], experimental data extracted at PSI by using ^{208}Pb have yielded an upper limit $R_{\mu e}^{\mathrm{Pb}} < 4.6\times 10^{-11}$. This experiment was an improvement by an order of magnitude over the previous upper limit, $R_{\mu e}^{\mathrm{Pb}} < 4.9\times 10^{-10}$, extracted from preliminary experimental data for the same target at TRIUMF [2].

The experimental sensitivity is expected to be further improved by two to three orders of magnitude by ongoing experiments at PSI (to 10^{-14}) [1], at TRIUMF (to 10^{-14}) [2,8], and at INS (to 10^{-14}–10^{-16}) [11]. Hopefully, such experiments will not only yield a still better limit, but they will detect some (μ^-,e^-) events which will signal the breakdown of the muon number conservation, revealing ''new physics'' beyond the standard model. For a discussion of lepton flavor violation limits in conjunction with theoretical predictions, the reader is referred to the recent survey by Depommier and Leroy [8].

Because of the similarity of electrons and muons, μ-e conversion was originally expected to proceed very fast. From a theoretical point of view, the basic background for the (μ^-,e^-) was set a long time ago by Weinberg and Feinberg [5] who assumed that this process is mediated by virtual photons [Fig. 1(a)]. Nonphotonic contributions [Fig. 1(b)–1(d)] were included later on in the post-gauge-theory era (for a recent review on this topic see Ref. [10] and for the experimental data extracted from various targets see Ref. [12]).

One expects that the Z-exchange diagrams, Figs. 1(b) and 1(c), to be less important than the W-box diagrams, Fig. 1(d), even for the incoherent process. The precise value depends, of course, on details like quark masses, etc. One also expects the W box to dominate by large factors especially in the case of heavy intermediate neutrinos [13]. Similar conclusions have been obtained by Marciano and Sanda [14]. In the present work we have not included exotic particles like Z' [15], exotic Higgs scalars, many Higgs doublets, R-parity-violating interactions, etc., which may in some models be important. We intentionally stayed within the context of the minimal extensions of the standard model, keeping also in mind that our emphasis here is on the nuclear structure aspects.

An interesting feature of the (μ^-,e^-) conversion in nuclei is the possibility of the ground-state to ground-state transitions. The strength of this channel is expected to be enhanced because of the coherent contribution of all nucleons of the participating nucleus or at least all protons. The rate for such transitions can be expressed in terms of the proton and neutron nuclear form factors [6,7,16]. Earlier estimates for the branching ratio $R_{\mu e}$ by Weinberg and Feinberg [5] have indicated that, for $A \geqslant 100$, this ratio is approximately constant, while Shanker [6] found that the ratio $R_{\mu e}$ could be larger in heavy nuclei.

The incoherent rate is much harder to calculate. The first such calculations have been performed only recently [9,17] in nuclei with closed (sub)shells throughout the periodic

*Permanent address: Theoretical Physics Division, University of Ioannina, GR 451 10, Greece.

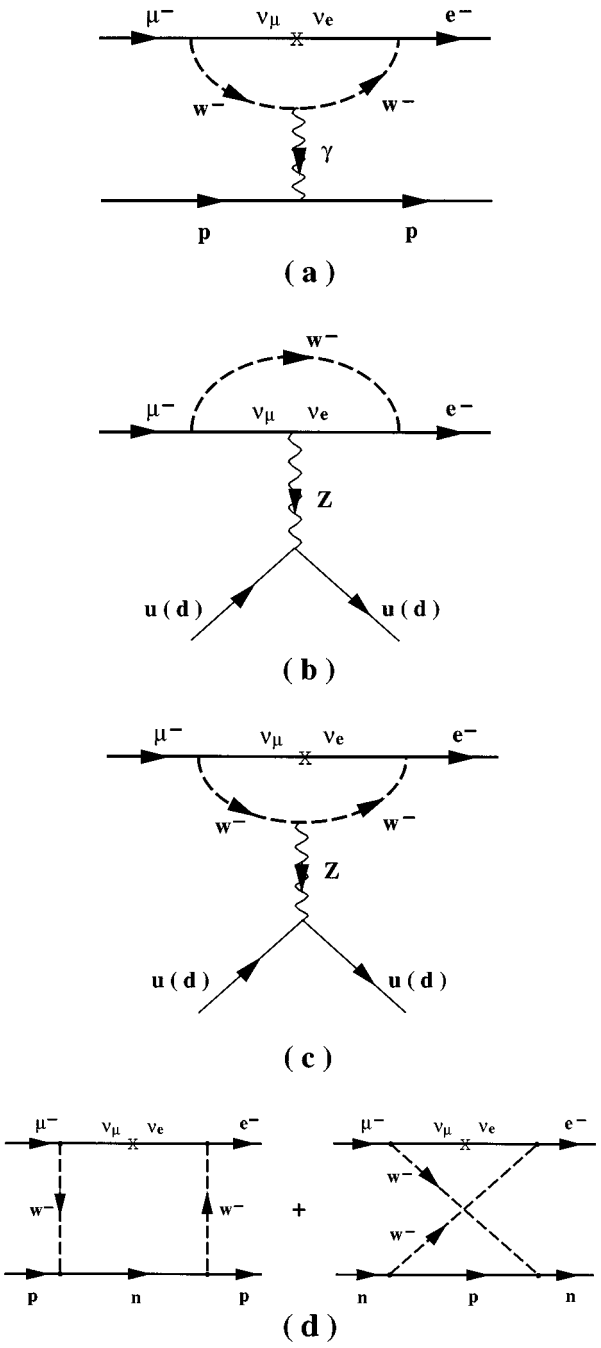

FIG. 1. Typical diagrams entering the (μ^-,e^-) conversion: the photonic (a), Z-exchange (b),(c), and box (d) diagrams. Only the specific mechanism involving intermediate neutrinos is exhibited here. $\nu_e=\Sigma_j U_{ej}\nu_j$, $\nu_\mu=\Sigma_j U_{\mu j}\nu_j$, where ν_j are the neutrino mass eigenstates and U_{ej}, $U_{\mu j}$ are the charge-lepton current-mixing matrix elements. Other mechanisms can also contribute (SUSY, Z', Higgs, etc.; see Ref. [10]).

table by employing shell model sum rules, i.e., by invoking closure approximation in some form with a suitable choice of a mean excitation energy, using a single Slater determinant for the initial state. In reality, these calculations give the total rate. The incoherent strength can be estimated by subtracting from the total strength the coherent part obtained independently. What, however, is needed is the ratio of the coherent rate to the total rate. Shell model results showed that the coherent channel dominates the (μ^-,e^-) process for light and medium nuclei, but in the region of ^{208}Pb, a great part of the rate comes from the inelastic channels. Furthermore, these calculations showed that the dependence of the branching ratio $R_{\mu e}$ on the nuclear mass A and charge Z reaches a maximum around $A\sim 100$ in agreement with the estimates of Ref. [5].

Recently [18], we have employed, for the coherent and incoherent (μ^-,e^-) conversion, another approach based on a local density approximation in conjunction with a relativistic Lindhard function for the description of the elementary processes: $\mu^- p\rightarrow e^- p$ and $\mu^- n\rightarrow e^- n$. The incoherent rate in this method was obtained by integrating over the excited states of a local Fermi sea. These results have shown that the coherent contribution is dominant for all nuclei and that the branching ratio $R_{\mu e}$ presents a maximum in the region of very heavy nuclei, i.e., in the Pb region.

In yet another recent theoretical study of the (μ^-,e^-) conversion [19], the quasiparticle random phase approximation (QRPA) was employed for the construction of the final nuclear states entering the coherent and incoherent rate. Such quasiparticle RPA results for ^{48}Ti have shown that the coherent channel dominates. One of the advantages of the QRPA method is that it can be used to estimate the mean excitation energy of the nucleus of interest, which in turn is useful in checking the results of the above-mentioned closure approximation which are sensitive to this property. The important result [19] was that the mean excitation energy $\overline{E}$ of the nucleus in process (1) is very small, $\overline{E}\approx 1$ MeV, which is appreciably smaller than $\overline{E}\approx 20$ MeV used in shell model calculations [9]. The latter value had been chosen from the phenomenology of the charge-changing (μ^-,ν_μ) reaction. This difference is mainly due to the fact that the coherent elastic channel, possible only in the (μ^-,e^-), is the dominant channel.

From the above discussion it is clear that a detailed study of all possible channels of the (μ^-,e^-) conversion for medium and heavy nuclei and in particular for nuclei around ^{208}Pb, which is of current experimental interest, is needed. In the present work, we use the formalism developed in the context of the quasiparticle RPA [19] (improved in the part of the reduced matrix elements; see the Appendix) to extend our previous results for ^{48}Ti and we report calculations performed for all individual (μ^-,e^-) conversion channels, in a set of isotopes covering the above region (see Table I, below) including, of course, ^{48}Ti and ^{208}Pb, since, the upper limit on the branching ratio $R_{\mu e}$ has been extracted [1–4] from experimental data on these nuclei. We note that the method using a local density approximation [18] cannot give us the individual contribution of each accessible channel.

Before embarking on such calculations, we mention that for certain nuclei, in particular those with closed shells like ^{60}Ni and ^{208}Pb, a special treatment in the QRPA is required in order to determine the pairing parameters for protons $(g^p_{\rm pair})$ and neutrons $(g^n_{\rm pair})$. In this work we follow the manner used recently in the double-beta decay [20]. In Sec. II we briefly discuss the method used, while the obtained results are presented and discussed in Sec. III and the conclusions are summarized in Sec. IV.

II. BRIEF DESCRIPTION OF THE METHOD

A. (μ^-,e^-) conversion effective operator

The effective Hamiltonian operator of the (μ^-,e^-) conversion, which involves both vector and axial vector currents, after the usual nonrelativistic reduction takes the form [10]

$$\Omega_V=\tilde{g}_V\sum_{j=1}^{A}(3+f_V\beta\tau_{3j})e^{-i\mathbf{q}\cdot\mathbf{r}_j},$$

$$\Omega_A=-\tilde{g}_A f_A\sum_{j=1}^{A}(\xi+\beta\tau_{3j})\frac{\sigma_j}{\sqrt{3}}e^{-i\mathbf{q}\cdot\mathbf{r}_j}. \tag{3}$$

The parameters $\tilde{g}_V$, $\tilde{g}_A$, and β depend on the assumed mechanism for lepton flavor violation [7,10]. For the photonic mechanism these parameters take the values $\tilde{g}_V=1/6$, $\tilde{g}_A=0$, $\beta=3$, and $f_V=1$, while, for the nonphotonic-neutrino-mediated mechanism, they are $\tilde{g}_V=\tilde{g}_A=1/2$, $\beta=5/6$, $f_V=1$, $f_A=1.24$, and $\xi=f_V/f_A=1/1.24$.

In Eq. (3), $\mathbf{q}$ represents the momentum transfer to the nucleus. Its magnitude is approximately given by

$$q=|\mathbf{q}|=m_\mu-\epsilon_b-(E_f-E_{\text{g.s.}}), \tag{4}$$

where m_μ is the muon mass, ϵ_b is the muon binding energy, and E_f and $E_{\text{g.s.}}$ are the energies of the final and ground state of the nucleus, respectively. We should mention that ϵ_b, although negligible in light nuclei, can become important in heavy elements (see Sec. III).

The matrix elements of the operators of Eq. (3) can be obtained via the multipole operators $T_M^{(l,s)J}$ given in the Appendix (for details see Refs. [10,19]).

B. Nuclear matrix elements for the coherent rate

In the case of the coherent (μ^-,e^-) process, i.e., ground-state to ground-state transitions $(0^+\to0^+)$, only the vector component of the (μ^-,e^-) operator contributes and the coherent rate is proportional to [10]

$$|\langle f|\Omega(q)|i,\mu\rangle|^2$$

$$=\tilde{g}_V^2(3+f_V\beta)^2\left[\tilde{F}_p(q^2)+\frac{3-f_V\beta}{3+f_V\beta}\tilde{F}_n(q^2)\right]^2, \tag{5}$$

where

$$\tilde{F}_{p,n}(q^2)=\int d^3x\rho_{p,n}(\mathbf{x})e^{-i\mathbf{q}\cdot\mathbf{x}}\Phi_\mu(\mathbf{x}). \tag{6}$$

In the last equation $\rho_p(\mathbf{x})$ and $\rho_n(\mathbf{x})$ represent the proton and neutron densities normalized to Z and N, respectively and $\Phi_\mu(\mathbf{x})$ is the muon wave function. If we assume that the muon is bound in the $1s$ atomic orbit which varies very little inside the nucleus, we can factorize the muon wave function out of the integral of Eq. (6) and write

$$\tilde{F}_p(q^2)\approx\langle\Phi_{1s}\rangle ZF_Z(q^2),\quad \tilde{F}_n(q^2)\approx\langle\Phi_{1s}\rangle NF_N(q^2), \tag{7}$$

where F_Z (F_N) is the usual proton (neutron) nuclear form factor.

We should mention that, experimentally, the most interesting quantities are the branching ratio $R_{\mu e}$ and the ratio η of the coherent to the total (μ^-,e^-) conversion rate [see Eq. (15), below]. We do not expect the branching ratio to be greatly affected by the approximation of Eq. (7), especially if we calculate the total μ^- capture rate in the same way. We expect this to be good even if for the total muon capture rate we use the Primakoff function [21], which is obtained by explicitly using this approximation. The Primakoff function fits the experimental data remarkably well throughout the periodic table (even for heavy nuclei). Furthermore, and for similar reasons, we expect that the ratio η is not going to be drastically affected by this approximation.

In the above approximation the nuclear dependence of the rate for the coherent process is proportional to the matrix element

$$M_{\text{coh}}^2(q^2)\equiv M_{\text{g.s.}\to\text{g.s.}}^2(q^2)$$
$$=\left[1+\frac{3-f_V\beta}{3+f_V\beta}\frac{N}{Z}\frac{F_N(q^2)}{F_Z(q^2)}\right]^2$$
$$\times Z^2F_Z^2(q^2). \tag{8}$$

Thus, the variation of the coherent (μ^-,e^-) conversion rate through the periodic table can be studied by calculating the matrix elements $M_{\text{g.s.}\to\text{g.s.}}^2$ of Eq. (8) for various A and Z. The nuclear form factors involved in $M_{\text{g.s.}\to\text{g.s.}}^2$ can either be calculated by using various models as the shell model [16,22], quasiparticle RPA [19,23], etc., or can be obtained directly from experiment whenever possible [24,25].

In the context of the quasiparticle RPA with an uncorrelated vacuum as the ground state, the nuclear form factors are given by (see the Appendix)

$$F_\tau(q^2)=\frac{1}{\tau}\sum_j (V_j^\tau)^2(2j+1)\langle j|j_0(qr)|j\rangle,\quad \tau=Z,N, \tag{9}$$

where $(V_j^\tau)^2$ are the occupation probabilities for the proton and neutron single-particle states $|j\rangle$ included in the used model space $[j\equiv(n,l,j)]$.

We should mention that, in the photonic case $(\beta=3)$, only the protons of the considered nucleus contribute and the right-hand side of Eq. (8) becomes $Z^2F_Z^2(q^2)$.

C. Incoherent rate by explicit calculations of the final states

The incoherent (μ^-,e^-) conversion rate is evaluated by summing the partial rates for all final nuclear states $|f\rangle$ except the ground state. We need calculate the matrix elements for both the vector and axial vector operators of Eq. (3), i.e., the quantities

$$S_\alpha=\sum_f\left(\frac{q_f}{m_\mu}\right)^2\int\frac{d\hat{\mathbf{q}}_f}{4\pi}|\langle f|\Omega_\alpha|\text{g.s.}\rangle|^2,$$

$$|f\rangle\neq|\text{g.s.}\rangle,\quad \alpha=V,A \tag{10}$$

($\hat{\mathbf{q}}_f$ is the unit vector in the direction of the momentum transfer $\mathbf{q}_f$).

As we have mentioned in the Introduction, for the calculation of S_V and S_A, one can either use the closure approximation [in which case the state $|f\rangle=|\text{g.s.}\rangle$ is included in Eq. (10)] or compute, state by state, the partial rates involved if one can construct the final states $|f\rangle$ in the context of some nuclear model. By using the multipole expansion operators $\hat{T}^{(l,\sigma)J}$ (see the Appendix), the matrix elements S_V and S_A are written as

$$S_\alpha=\sum_{f_{\text{exc}}}\left(\frac{q_{\text{exc}}}{m_\mu}\right)^2\sum_{l,J}\ |\langle f_{\text{exc}}||\hat{T}^{(l,\sigma)J}||\text{g.s.}\rangle|^2 \tag{11}$$

[$\alpha=V,A$, for the vector ($\sigma=0$) and axial vector ($\sigma=1$) components, respectively]. The partial matrix element from the initial state 0^+ to an excited state $|f\rangle$ in the context of the QRPA takes the form

$$\langle f||\hat{T}^{(l,\sigma)J}||0^+\rangle=\sum_{\lambda,\tau}\ W_\lambda^J[X_\lambda^{(f,J,\tau)}U_{j_2}^{(\tau)}V_{j_1}^{(\tau)}+Y_\lambda^{(f,J,\tau)}V_{j_2}^{(\tau)}U_{j_1}^{(\tau)}], \tag{12}$$

where $V_j^{(\tau)}$ and $U_j^{(\tau)}$ represent the probability amplitudes for the single-particle states to be occupied and unoccupied, respectively. They are determined by solving the BCS equations iteratively. X and Y represent the forward and backward scattering amplitudes. They are obtained by solving the QRPA equations. The index λ runs over two-particle configurations coupled to a given J, namely, $(j_1,j_2)J$ for the proton ($\tau=1$) or neutron ($\tau=-1$). The quantities $W_\lambda^J\equiv W_{j_2j_1}^J$ are given in the Appendix.

For the total (μ^-,e^-) rate the relevant matrix elements are obtained by adding the vector and axial vector contributions of the coherent and incoherent rate, i.e.,

$$M_{\text{tot}}^2=S_V+3S_A+S_0, \tag{13}$$

where S_0 is associated with the ground-state–to–ground-state transition,

$$S_0=\left(\frac{q_{\text{g.s.}}}{m_\mu}\right)^2\sum_{l,J}\ |\langle\text{g.s.}||\hat{T}^{(l,\sigma)J}||\text{g.s.}\rangle|^2, \tag{14}$$

for the vector component $\sigma=0$ and for the axial vector component $\sigma=1$. For 0^+ nuclei only the vector term contributes.

III. RESULTS AND DISCUSSION

Using the method outlined above, in the present work we have calculated the matrix elements needed for both the coherent and incoherent (μ^-,e^-) rates, for the nuclei ^{48}Ti, ^{60}Ni, ^{72}Ge, ^{112}Cd, ^{162}Yb, and ^{208}Pb. The specific parameters used and a brief description of the model spaces employed can be read from Table I. For all nuclei considered we have employed the same model space for protons and neutrons. For the harmonic oscillator parameter b in the region of heavy nuclei we have employed the improved expressions of Ref. [26].

In the BCS description of the uncorrelated ground state, for each nuclear isotope the single-particle energies have been calculated from a Coulomb corrected Woods-Saxon potential with spin-orbit coupling. The G-matrix elements of the realistic Bonn one-boson-exchange potential [27] have been employed. The values of the pairing parameters g_{pair}^p and g_{pair}^n renormalizing the proton and neutron pairing channels in the G matrix have been deduced by comparing the quasiparticle energies with experimental pairing gaps as is described in Refs. [28,29]. For the special cases of $^{60}_{28}$Ni, which is a proton closed-shell nucleus, and $^{208}_{82}$Pb, which is a doubly closed-shell nucleus, the pairing parameters have been deduced from the neighboring nuclei $^{60}_{26}$Fe and $^{208}_{84}$Po, respectively, in analogy with the procedure followed in the study of the nuclear double-beta decay in the double closed-shell nucleus $^{48}_{20}$Ca [20]. The resulting pairing parameters g_{pair}^p and g_{pair}^n for each nucleus are shown in Table I.

A. Coherent process

It is obvious from Eq. (8) that, for the coherent process, i.e., g.s.→g.s. transitions, we need the proton and neutron

TABLE I. Renormalization constants for proton (g_{pair}^p) and neutron (g_{pair}^n) pairing interactions determined from the experimental proton (Δ_p^{expt}) and neutron (Δ_n^{expt}) pairing gaps.

Nucleus	Configuration space	b_{HO}(fm^{-1})	Δ_p^{expt}(MeV)	Δ_n^{expt}(MeV)	g_{pair}^p	g_{pair}^n
$^{48}_{22}$Ti$_{26}$	16 levels (no core)	1.92	1.896	1.564	1.082	1.002
$^{60}_{28}$Ni$_{32}$	16 levels (no core)	2.02	1.718 [a]	1.395 [a]	1.033	0.901
$^{72}_{32}$Ge$_{40}$	16 levels (no core)	2.07	1.611	1.835	0.924	0.995
$^{112}_{48}$Cd$_{64}$	16 levels (core $^{40}_{20}$Ca$_{20}$)	2.21	1.506	1.331	1.099	0.950
$^{162}_{70}$Yb$_{92}$	23 levels (core $^{40}_{20}$Ca$_{20}$)	2.32	1.170	1.104	0.894	0.951
$^{208}_{82}$Pb$_{126}$	18 levels (core $^{100}_{50}$Sn$_{50}$)	2.40	0.807 [a]	0.611 [a]	0.861	1.042

[a]For the closed-shell nuclei the parameters g_{pair}^p and g_{pair}^n have been borrowed from the $(N\pm2,Z\mp2)$ nuclei; i.e., the experimental gaps (columns 4 and 5) for $^{60}_{28}$Ni$_{32}$ and $^{208}_{82}$Pb$_{126}$ are those of $^{60}_{26}$Fe$_{34}$ and $^{208}_{84}$Po$_{124}$, respectively.

TABLE II. Nuclear form factors for protons (F_Z) and neutrons (F_N) calculated in the context of the shell model [9] and quasiparticle RPA cases QRPA(i) and QRPA(ii) (see text). For comparison the experimental form factors [24,25] are also shown.

Nucleus	Shell model			QRPA(i)		QRPA(ii)			Expt.
(A,Z)	$b_{\rm HO}$ (fm^{-1})	F_Z	F_N	F_Z	F_N	ϵ_b (MeV)	F_Z	F_N	$F_Z^{\rm expt}$
$^{48}_{22}$Ti$_{26}$	1.906	0.543	0.528	0.528	0.506	1.250	0.537	0.514	0.532
$^{60}_{28}$Ni$_{32}$	1.979	0.489	0.478	0.489	0.476	1.950	0.503	0.490	0.494
$^{72}_{32}$Ge$_{40}$	2.040	0.470	0.448	0.456	0.435	2.150	0.472	0.451	0.443
$^{112}_{48}$Cd$_{64}$	2.202	0.356	0.318	0.349	0.312	4.890	0.388	0.352	0.353
$^{162}_{70}$Yb$_{92}$	2.335	0.261	0.208	0.252	0.218	8.445	0.314	0.280	0.305
$^{208}_{82}$Pb$_{126}$	2.434	0.194	0.139	0.207	0.151	10.475	0.271	0.214	0.242

nuclear form factors $F_Z(q^2)$ and $F_N(q^2)$, respectively. The results, obtained by using as the ground state the uncorrelated RPA vacuum, are listed in Table II for the following two cases.

(i) By neglecting the muon binding energy ϵ_b in Eq. (4) (as in Refs. [5,9]). Then, the elastic momentum transfer is the same for all nuclei, i.e., $q \approx m_\mu \approx 0.535$ fm^{-1}. Such results are indicated as QRPA(i).

(ii) By taking into account ϵ_b in Eq. (4). Then, the elastic momentum transfer is $q \approx m_\mu - \epsilon_b$ and varies from $q \approx 0.529$ fm^{-1}, for ^{48}Ti where $\epsilon_b \approx 1.3$ MeV, to $q \approx 0.482$ fm^{-1}, for ^{208}Pb where $\epsilon_b \approx 10.5$ MeV [see Table II, results indicated as QRPA(ii)].

In Table II we also present the shell model results of Ref. [9], obtained with $q = 0.535$ fm^{-1} throughout the periodic table, i.e., as in case (i) above. We see that QRPA(i) and shell model methods give about the same results. However, the form factors of QRPA(ii) for heavy nuclei differ appreciably from those of both QRPA(i) and the shell model. For ^{208}Pb, for example, the QRPA(ii) form factors are about 30% larger than the corresponding QRPA(i) and shell model. This happens because the inclusion of ϵ_b results in a smaller momentum transfer to the nucleus and, consequently, in an increase of the form factors. The larger the value of ϵ_b, lead region, the larger the difference between form factors QRPA(i) and QRPA(ii).

In Table II we also show the experimental form factors obtained from electron scattering data [24,25] at momentum transfer $q = m_\mu - \epsilon_b$. We see that, when using the right form factors, i.e., taking into account the binding energy ϵ_b [QRPA(ii) case], the form factors calculated in the present work, are in good agreement with the experimental ones. The deviation is less than 5% with the possible exception of ^{112}Cd and ^{208}Pb where it is about 10%.

The variation of the coherent nuclear matrix elements $M^2_{\rm coh}$ with respect to A and Z is shown in Fig. 2(a), for the photonic mechanism, and Fig. 2(b), for the nonphotonic one. From these figures we see that, by taking into account the muon binding energy ϵ_b, QRPA(ii), all matrix elements increase continuously up to the lead region where they become about a factor of 2 larger than the corresponding QRPA(i) and shell model values. This implies that the coherent rate becomes larger for the heavy nuclei, Pb region, which makes such nuclei attractive from an experimental point of view [2,4] provided, of course, that they also satisfy other additional criteria, e.g., the minimization of the reaction background, etc. [8,12]. The (μ^-,e^-) conversion electrons of a given target are expected to show a pronounced peak around $E_e = m_\mu - \epsilon_b$, which for the lead region is $E_e \approx 95$ MeV. One prefers this peak to be as far as possible above the reaction-induced background.

We should recall that, in the present work and in the shell model method of Ref. [9], the factorization approximation, Eq. (7), was used. The exact expression, Eq. (6), was used in Ref. [18] and yielded matrix elements which for heavy nuclei are larger than the approximate ones. This, however, as we have extensively seen in Sec. II B, only slightly affects the branching ratio $R_{\mu e}$ and the ratio η of the coherent rate to the total rate, which in our case are the most important quantities. We also mention that shell model results for the total muon capture rate [31], obtained by using the exact muon wave function, differ by only 5.7%, in the case of ^{60}Ni, and by 7.0%, in the case of ^{208}Pb, from those obtained by using the approximation of Eq. (7). Detailed QRPA calculations, which do not invoke this factorization approximation, are under way and will be published elsewhere.

B. Incoherent process

As we have stated in Sec. II C, the incoherent process in the present work is investigated by calculating, state by state, the contributions of all the excited states of the nucleus in question which are included in the model space described in Table I.

For the photonic mechanism the nuclear matrix elements obtained for all positive and negative parity states up to 6^- and 6^+ are shown in Table III. For this mechanism only the vector component S_V gives a nonzero contribution ($M^2_{\rm inc} = S_V$). For the nonphotonic mechanism we have non-

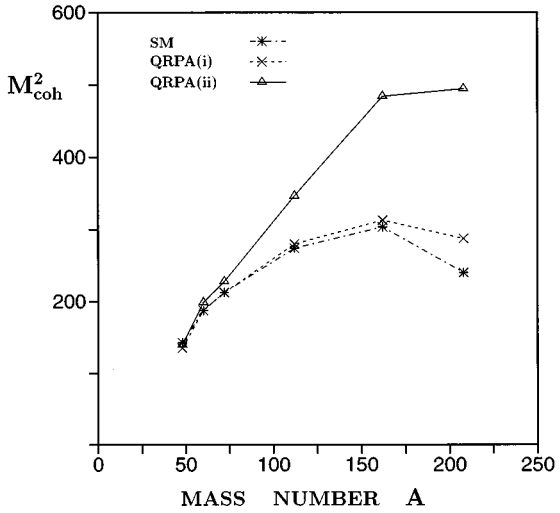

FIG. 2. Variation of the coherent (μ^-,e^-) conversion matrix elements $M^2_{\rm coh}$ for specific mass A and charge Z (see text) for the photonic mechanism (a) and the nonphotonic mechanism (b). In QRPA(i) the muon binding energy ϵ_b was neglected, but it was included in QRPA(ii). We see that ϵ_b strongly affects the matrix elements for heavy nuclei. For comparison the results of Ref. [9] (shell model results) are also shown. For photonic and nonphotonic diagrams the coherent rate increases up to the *Pb* region where it starts to decrease.

zero contributions from both the vector and axial vector components S_V and S_A, and the results are shown in Table IV ($M^2_{\rm inc}=S_V+3S_A$).

From Tables III and IV we see that the main contribution to the incoherent rate comes from the low-lying excited states. High-lying excited states contribute negligibly. This means that for a given A, a nuclear isotope with many low-lying states in its spectrum is characterized by large incoherent matrix elements.

For the doubly closed-shell nucleus ^{208}Pb, which is of current experimental interest [2,4], the incoherent matrix elements are smaller than expected. A plausible explanation is that the spectrum of this nucleus presents a large gap (minimum energy needed to excite the first excited state) and only few excited states lie below ≈ 5 MeV.

TABLE III. Incoherent μ-e conversion matrix elements ($M^2_{\rm inc}$) for the photonic mechanism. Only the vector component (S_V) of the operator of Eq. (3) contributes.

J^π	$^{48}_{22}$Ti	$^{60}_{28}$Ni	$^{72}_{32}$Ge	$^{112}_{48}$Cd	$^{162}_{70}$Yb	$^{208}_{82}$Pb
0^+	1.946	1.160	2.552	2.088	4.305	2.512
2^+	0.242	0.738	1.396	2.669	6.384	2.342
4^+	0.004	0.005	0.015	0.021	0.063	0.056
6^+	6×10^{-6}	6×10^{-6}	1×10^{-5}	6×10^{-5}	2×10^{-4}	3×10^{-4}
1^-	3.711	4.215	5.066	5.282	4.824	4.533
3^-	0.037	0.081	0.152	0.249	0.542	0.476
5^-	2×10^{-4}	2×10^{-4}	5×10^{-4}	0.001	0.005	0.005
S_V	5.940	6.199	9.181	10.309	16.123	9.924
$M^2_{\rm inc}$	5.940	6.199	9.181	10.309	16.123	9.924

In general, the incoherent matrix elements do not show clear A and Z dependence. Their magnitude depends on the spectrum of the individual nuclear isotope.

In obtaining the results of Tables III and IV for 1^- states, we removed the spurious center-of-mass contributions by ex-

TABLE IV. Nonphotonic mechanism. Incoherent μ-e conversion matrix elements ($M^2_{\rm inc}$) for the vector (S_V) and axial vector (S_A) components of the (μ^-,e^-) operator.

J^π	$^{48}_{22}$Ti	$^{60}_{28}$Ni	$^{72}_{32}$Ge	$^{112}_{48}$Cd	$^{162}_{70}$Yb	$^{208}_{82}$Pb
0^+	2.245	1.441	3.326	3.006	6.097	4.106
2^+	0.363	1.000	1.899	4.869	12.618	3.769
4^+	0.002	0.006	0.017	0.029	0.078	0.070
6^+	2×10^{-6}	7×10^{-6}	1×10^{-6}	8×10^{-5}	2×10^{-4}	4×10^{-4}
1^-	4.010	6.164	6.676	7.243	6.796	5.537
3^-	0.059	0.097	0.177	0.328	0.684	0.572
5^-	1×10^{-4}	2×10^{-4}	5×10^{-4}	0.002	0.006	0.006
S_V	6.679	8.708	12.095	15.477	26.280	14.061
1^+	0.265	1.114	0.795	0.943	1.599	0.951
2^+	0.041	0.189	0.208	0.362	0.644	0.466
3^+	0.044	0.221	0.244	0.422	0.693	0.635
4^+	2×10^{-4}	0.001	0.002	0.005	0.013	0.015
5^+	2×10^{-4}	0.002	0.002	0.007	0.013	0.021
6^+	1×10^{-7}	1×10^{-6}	1×10^{-7}	1×10^{-5}	4×10^{-5}	9×10^{-5}
0^-	0.770	1.498	1.394	1.840	1.925	1.539
1^-	0.594	1.149	1.057	1.394	1.072	0.616
2^-	0.673	0.800	0.880	1.035	1.137	1.170
3^-	0.010	0.015	0.024	0.050	0.091	0.110
4^-	0.009	0.019	0.031	0.057	0.164	0.129
5^-	8×10^{-6}	2×10^{-5}	6×10^{-5}	2×10^{-4}	0.001	0.001
6^-	9×10^{-6}	7×10^{-5}	1×10^{-4}	3×10^{-4}	0.001	0.001
$3S_A$	2.405	5.009	4.637	6.115	7.305	6.226
$M^2_{\rm inc}$	9.084	13.717	16.732	21.592	33.585	20.287

TABLE V. Coherent and total μ-e conversion rate matrix elements QRPA(ii) (see text) for the photonic mechanism in the neutrino-mediated process. For comparison, we also show the ratio η of Eq. (15) given by the shell model [9] obtained by ignoring the muon binding energy ϵ_b. The results of QRPA(i) are similar to those of the shell model.

Nucleus	QRPA(ii) Matrix elements		η%	
(A,Z)	$M^2_{\text{g.s.}\to\text{g.s.}}$	M^2_{tot}	QRPA(ii)	Shell model
$^{48}_{22}\text{Ti}_{26}$	139.6	145.5	95.9	
$^{60}_{28}\text{Ni}_{32}$	198.7	204.9	96.9	64.9
$^{72}_{32}\text{Ge}_{40}$	227.8	237.0	96.1	59.7
$^{112}_{48}\text{Cd}_{64}$	346.7	357.0	97.1	
$^{162}_{70}\text{Yb}_{92}$	484.3	500.4	96.8	36.9
$^{208}_{82}\text{Pb}_{126}$	494.7	504.6	98.0	25.5

plicitly calculating the spurious state $|S\rangle$ and removing its admixtures from the incoherent and total rate. We have also calculated the overlaps $\langle 1^-,m|S\rangle$ (where m counts the 1^- excited states) and found that most of the spuriousity lies in the lowest 1^- state, being 88% for ^{48}Ti, 63% for ^{60}Ni, 62% for ^{72}Ge, 57% for ^{112}Cd, 87% for ^{162}Yb, and 77% for ^{208}Pb [30]. We should stress that, for all nuclei studied, the spurious center-of-mass contribution is less than 30% of the incoherent matrix elements, i.e., 1.0–1.5 % of the total (μ^-,e^-) conversion rate.

An additional point we should note is the effect of the ground-state correlations on the (μ^-,e^-) matrix elements. In the QRPA this can be easily estimated by using a correlated quasiparticle RPA vacuum instead of the uncorrelated one [32–35]. In the present work we have not performed additional calculations with a correlated RPA vacuum. It is known, however, that the matrix elements for ^{48}Ti obtained this way [19] are reduced by $\approx$30%. The ground-state correlations tend to decrease the strengths of all (μ^-,e^-) conversion channels, but do not affect the parameter η (see Sec. III C).

C. Comparison of coherent and incoherent processes

As we have seen above, the g.s.$\to$g.s. channel is the most important one. Therefore, a useful quantity for the (μ^-,e^-) conversion is the fraction of the coherent matrix elements M^2_{coh} divided by the total one M^2_{tot}, i.e., the ratio

$$\eta = M^2_{\text{coh}}/M^2_{\text{tot}}. \tag{15}$$

In earlier calculations η was estimated [5] to be a decreasing function of A with a value of $\eta\approx 83\%$ in the Cu region. By using, however, the most appropriate QRPA(ii) results, we find that indeed the coherent channel dominates throughout the periodic table (see Table V for the photonic and Table VI for the nonphotonic mechanisms). In fact we see that the values of η obtained in the present calculations are a bit larger than those of Ref. [18] obtained with a local density approximation and a lot larger than those of Ref. [9]. We should stress, however, that the exaggeration of the incoherent channels in the shell model calculations of Ref. [9] is not a shortcoming of the method itself but the result of ignoring the muon binding energy ϵ_b in calculating the nuclear form factors. In fact, repeating the calculations of Ref. [9] and taking into account the effect of ϵ_b on the form factors of the coherent process as well as on the mean excitation energy entering the total rate, we find a value of $\eta\geqslant 75\%$.

IV. CONCLUSIONS

In the present work we have studied in detail the dependence of (μ^-,e^-) conversion matrix elements on the nuclear parameters A and Z. Our nuclear matrix elements were obtained in the context of quasiparticle random phase approximation (QRPA) which permits a relatively simple construction of all needed final states. So there was no need to invoke a closure approximation. The results obtained cover six nuclear systems from ^{48}Ti to ^{208}Pb, which are of experimental interest. The most important conclusions stemming out of our detailed study are the following.

(i) The coherent mode dominates throughout the periodic table but it is more pronounced in the heavy nucleus ^{208}Pb which is currently used at PSI in the SINDRUM II experiment.

(ii) The coherent and total rates as well as the ratio η (coherent to total) tend to increase as a function of the mass number A up to the Pb region. This encourages the use of heavier nuclear targets to look for lepton flavor violation.

(iii) In evaluating the nuclear matrix elements the muon binding energy should not be ignored especially for heavy nuclear elements.

(iv) The great part of the incoherent rate comes from the low-lying excitations.

The results obtained in the present work are in good agreement with those obtained in the framework of the local density approximation as well as those of shell model calcu-

TABLE VI. The same as in Table V for a nonphotonic mechanism ($\beta=5/6$) in the neutrino-mediated process. For comparison we have added the results for η obtained with a local density approximation (LDA) [18] and shell model [9].

Nucleus	QRPA(ii) Matrix elements		η%		
(A,Z)	$M^2_{\text{g.s.}\to\text{g.s.}}$	M^2_{tot}	QRPA(ii)	Shell model	LDA
$^{48}_{22}\text{Ti}_{26}$	375.2	384.3	97.6		91.0
$^{60}_{28}\text{Ni}_{32}$	527.4	541.1	97.5	74.9	
$^{72}_{32}\text{Ge}_{40}$	639.5	656.2	97.4	70.3	
$^{112}_{48}\text{Cd}_{64}$	983.3	1004.9	97.8		93.0
$^{162}_{70}\text{Yb}_{92}$	1341.2	1374.8	97.6	40.1	
$^{208}_{82}\text{Pb}_{126}$	1405.2	1425.5	98.5	28.2	94.0

lations provided that all calculations take into account the muon binding energy ϵ_b.

ACKNOWLEDGMENTS

This work has been partially supported (T.S.K.) by DFG Grant No. FA67/19-1. The authors T.S.K. and J.D.V. would like to acknowledge support from the EU Human Capital and Mobility Program No. CHRX-CT 93-0323.

APPENDIX

(A) The multipole expansion operators $\hat{T}^{(l,\sigma)J}$, resulting from Ω_V and $\mathbf{\Omega}_A$ of Eq. (3), are written as

$$T_M^{(l,0)J}=\tilde{g}_V\delta_{lJ}\sqrt{4\pi}\sum_{i=1}^{A}(3+\beta\tau_{3i})j_l(qr_i)Y_M^l(\hat{\mathbf{r}}_i) \quad \text{(A1)}$$

for Ω_V, the spin-independent component, and

$$T_M^{(l,1)J}=\tilde{g}_A\sqrt{\frac{4\pi}{3}}\sum_{i=1}^{A}(\xi+\beta\tau_{3i})j_l(qr_i)[Y^l(\hat{\mathbf{r}}_i)\otimes\boldsymbol{\sigma}_i]_M^J \quad \text{(A2)}$$

for $\mathbf{\Omega}_A$, the spin-dependent component. $j_l(qr)$ are the spherical Bessel functions.

The quantities $W_\lambda^J\equiv W_{j_2j_1}^J$ of Eq. (12) contain the reduced matrix elements of the operators $\hat{T}^J$ between the single-particle proton or neutron states j_1 and j_2 as

$$W_{j_1j_2}^J(\tau)=(\zeta+\tau\beta)\frac{\langle j_1||\hat{T}^J||j_2\rangle}{2J+1} \quad \text{(A3)}$$

($\zeta=3$ for Ω_V and $\zeta=1/1.24$ for $\mathbf{\Omega}_A$). The reduced matrix elements $\langle j_1||T^J||j_2\rangle$ are given in Ref. [19]. The relevant radial matrix elements $\langle n_1l_1|j_l(qr)|n_2l_2\rangle$, for the harmonic oscillator basis often used, can be written in the elegant way

$$\langle n_1l_1|j_l(qr)|n_2l_2\rangle=e^{-\chi}\sum_{\kappa=0}^{\kappa_{\max}}\varepsilon_\kappa\chi^{\kappa+l/2},\quad \chi=(qb)^2/4, \quad \text{(A4)}$$

where

$$\kappa_{\max}=n_1+n_2+m,\quad m=(l_1+l_2-l)/2.$$

The coefficients $\varepsilon_\kappa(n_1l_1,n_2l_2,l)$, in general simple numbers, are given by

$$\varepsilon_\kappa=\left[\frac{\pi n_1!n_2!}{4\Gamma\left(n_1+l_1+\frac{3}{2}\right)\Gamma\left(n_2+l_2+\frac{3}{2}\right)}\right]^{1/2}\times\sum_{\kappa_1=\phi}^{n_1}\sum_{\kappa_2=\sigma}^{n_2}n!\Lambda_{\kappa_1}(n_1l_1)\Lambda_{\kappa_2}(n_2l_2)\Lambda_\kappa(nl), \quad \text{(A5)}$$

where the $\Lambda_\kappa(nl)$ are defined in Ref. [19], $n=\kappa_1+\kappa_2+m$, and

$$\phi=\begin{cases}0, & \kappa-m-n_2\leqslant 0,\\ \kappa-m-n_2, & \kappa-m-n_2>0,\end{cases}$$

$$\sigma=\begin{cases}0, & \kappa-m-\kappa_1\leqslant 0,\\ \kappa-m-\kappa_1, & \kappa-m-\kappa_1>0.\end{cases}$$

The advantage of Eq. (A4) is that it permits the calculation of ε_κ, which are independent of the momentum q, once and for the whole model space used. Afterwards, the relevant reduced matrix elements are easily obtained for every value of the momentum transfer q.

(B) In the context of the quasiparticle RPA, the point-proton (-neutron) nuclear form factors of Eq. (9) can be cast in the compact form

$$F_\tau(q^2)=\frac{1}{\tau}e^{-(qb)^2/4}\sum_{\lambda=0}^{N_{\text{space}}}\theta_\lambda^\tau(qb)^{2\lambda},\quad \tau=Z,N, \quad \text{(A6)}$$

where b is the harmonic oscillator parameter, N_{space} represents the maximum harmonic oscillator quanta included in the model space used (see Table I), and θ_λ^τ the coefficients

$$\theta_\lambda^\tau=\frac{\sqrt{\pi}}{2}\sum_{(n,l)j,\lambda\geqslant l}(V_j^\tau)^2\frac{(2j+1)n!C_{nl}^{\lambda-l}}{\Gamma(n+l+\frac{3}{2})}, \quad \text{(A7)}$$

where $(V_j^\tau)^2$ are the occupation probabilities for the proton (neutron) single-particle j levels. The coefficients C_{nl}^m are given in Ref. [22].

[1] SINDRUM II Collaboration, C. Dohmen *et al.*, Phys. Lett. B **317**, 631 (1993).

[2] TRIUMF Collaboration, S. Ahmad *et al.*, Phys. Rev. Lett. **59**, 970 (1987); Phys. Rev. D **38**, 2102 (1988).

[3] SINDRUM Collaboration, A. Badertscher *et al.*, J. Phys. G **17**, S47 (1991); A. van der Schaaf, Nucl. Phys. **A546**, 421c (1992); Prog. Part. Nucl. Phys. **31**, 1 (1993).

[4] SINDRUM II Collaboration, W. Honecker *et al.*, Phys. Rev. Lett. **76**, 200 (1996).

[5] S. Weinberg and G. Feinberg, Phys. Rev. Lett. **3**, 111 (1959); **3**, 244(E) (1959).

[6] O. Shanker, Phys. Rev. D **20**, 1608 (1979).

[7] J. D. Vergados, Phys. Rep. **133**, 1 (1986).

[8] P. Depommier and C. Leroy, Rep. Prog. Phys. **58**, 61 (1995).

[9] T. S. Kosmas and J. D. Vergados, Nucl. Phys. **A510**, 641 (1990).

[10] T. S. Kosmas, G. K. Leontaris, and J. D. Vergados, Prog. Part. Nucl. Phys. **33**, 397 (1994); T. S. Kosmas and J. D. Vergados, Phys. Rep. **264**, 251 (1996).

[11] MELC Collaboration, V.S. Abadjev *et al.*, report, INS/Moscow, 1992; V. M. Lobashev (private communication).

[12] D. A. Bryman *et al.*, Phys. Rev. Lett. **28**, 1469 (1972); **55**, 465 (1985); A. Badertscher *et al.*, Nucl. Phys. **A377**, 406 (1982).

[13] G. K. Leontaris, Ph.D. thesis, University of Ioannina, Greece, 1986.

[14] W. J. Marciano and A. I. Sanda, Phys. Rev. Lett. **38**, 1512 (1977).

[15] J. Bernabeu, E. Nardi, and D. Tommasini, Nucl. Phys. **B409**, 69 (1993).
[16] T. S. Kosmas and J. D. Vergados, Phys. Lett. B **215**, 460 (1988).
[17] T. S. Kosmas and J. D. Vergados, Phys. Lett. B **217**, 19 (1989).
[18] H. C. Chiang, E. Oset, T. S. Kosmas, A. Faessler, and J. D. Vergados, Nucl. Phys. **A559**, 526 (1993).
[19] T. S. Kosmas, J. D. Vergados, O. Civitarese, and A. Faessler, Nucl. Phys. **A570**, 637 (1994).
[20] J. Suhonen, J. Phys. G **19**, 139 (1993).
[21] B. Goulard and H. Primakoff, Phys. Rev. C **10**, 2034 (1974).
[22] T. S. Kosmas and J. D. Vergados, Nucl. Phys. **A523**, 72 (1992).
[23] T. S. Kosmas, A. Faessler, F. Šimkovic, and J.D. Vergados, in *Proceedings of the 5th Hellenic Symposium on Nuclear Physics*, Ioannina, 1993, edited by X. Aslanoglou *et al.* (Ioannina University Press, Ioannina, 1994), p. 216.
[24] J. Heisenberg, R. Hofstadter, J. S. McCarthy, and I. Sick, Phys. Rev. Lett. **23**, 1402 (1969); T. W. Donnelly and J. D. Walecka, Annu. Rev. Nucl. Sci. **25**, 329 (1975); B. Frois and C. N. Papanicolas, Annu. Rev. Nucl. Part. Sci. **37**, 133 (1987).
[25] H. de Vries, C. W. de Jager, and C. de Vries, At. Data Nucl. Data Tables **36**, 495 (1987).
[26] G. A. Lalazissis and C. P. Panos, Phys. Rev. C **51**, 1247 (1995).
[27] K. Holinde, Phys. Rep. **68**, 121 (1981).
[28] J. Suhonen, I. Taigel, and A. Faessler, Nucl. Phys. **A486**, 91 (1988).
[29] M. K. Cheoun, A. Bobyk, A. Faessler, F. Simkovic, and G. Teneva, Nucl. Phys. **A561**, 74 (1993); **A564**, 329 (1993).
[30] D. Duplain, B. Goulard, and J. Joseph, Phys. Rev. C **12**, 28 (1975).
[31] J. Schwieger, A. Faessler, and T. S. Kosmas, Phys. Rev. C (to be submitted).
[32] D.J. Rowe, *Nuclear Collective Motion* (Methuen, London, 1970).
[33] E. A. Sanderson, Phys. Lett. **19**, 141 (1965); J. Da Providencia, *ibid.* **21**, 668 (1966).
[34] P. J. Ellis, Nucl. Phys. **A467**, 173 (1987).
[35] J. A. McNeil, C. E. Price, and J. R. Shepard, Phys. Rev. C **42**, 2442 (1990).